ACS OMEGA

Open Access

http://pubs.acs.org/journal/acsodf

Article

Catalytic Performance Investigation of Alkali and Bifunctional Catalysts Derived from Lignocellulosic Biomasses for Biodiesel Synthesis from Waste Frying Oil

Demelash Tilahun Bekele, Nurelegne Tefera Shibeshi,* and Ali Shemsedin Reshad

Cite This: *ACS Omega* 2024, 9, 2815−2829

Read Online

ACCESS | Metrics & More | Article Recommendations

ABSTRACT: In this study, alkali and bifunctional catalysts were synthesized for waste frying oil methyl ester (WFOME) synthesis. Coffee husk (CH) and CH blended with *Eragrostis tef* straw (TS) (CH−TS) lignocellulosic biomasses (LBs) were utilized during the catalysts' synthesis. The alkali catalysts were CH and CH−TS ashes, both modified by KNO_3 impregnation. They are designated as C-45 and C-Mix, respectively. Zirconia (ZrO_2) promoted CH ash catalysts via precipitation followed by impregnation (Bic-PP) and in situ precipitation−impregnation (Bic-Dm) were the bifunctional ones. CH and CH−TS chars were the supporting frameworks during the catalysts' composite materials (CCMs) preparation. The combustion performance of LBs and CCMs was evaluated and associated with the catalysts' physicochemical properties. Using XRD, SEM, FTIR, alkalinity, TOF, and BET surface area analysis, catalysts were characterized. The combustion performance of the LBs was in the order of TS > CH−TS > CH. Among CCMs, the highest combustion performance was for CCM-Mix (KNO_3/(CH−TS char)) and the lowest was for CCM-45 (KNO_3/ CH char). The C-Mix catalyst was a light green powder due to the reaction between inorganic components, whereas C-45 was dark gray due to the presence of unburned char. The CCMs for bifunctional catalysts had moderate combustion performance and yielded light gray powdered catalysts containing tetragonal ZrO_2. The optimum WFOME yields were 98.08, 97, 92.69, and 93.05 wt % for C-Mix, C-45, Bic-Dm, and Bic-PP assisted WFO transesterification, respectively. The results were obtained at a reaction temperature of 65 °C, time of 1 h, and methanol to WFO molar ratio of 15:1 using catalyst amounts of 5 and 7 wt % for the alkali and bifunctional catalysts, respectively. The greatest moisture resistance was offered by the C-Mix catalyst. The best reusability was for the C-45 catalyst. Catalysts' deactivation modes include active site leaching and poisoning.

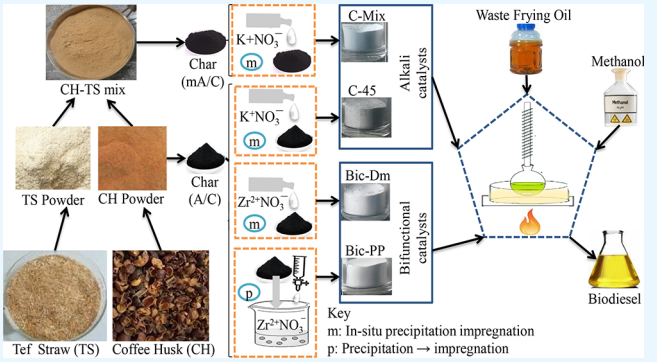

INTRODUCTION

In addition to lowering energy costs, producing energy from renewable resources makes the environment convenient for living. Currently, the transport sector uses the majority of the energy produced from fossil fuels, which is close to 80% of the total.[1] Therefore, investigating a facile method of biodiesel synthesis for petrodiesel substitution is a great contribution. Biodiesel is a viable renewable fuel because of its low toxicity, high flash point, low sulfur content, low toxicity, and environmentally friendly exhaust emissions.[2] One of the main topics in the biodiesel sector is the synthesis of appropriate catalysts for the transesterification of low-cost feedstocks.[3] Heterogeneous solid catalysts are the subject of current studies because they have many advantages including reusability and recyclability.[4]

Heterogeneous catalysts have drawbacks such as low strength, active site leaching, poor resistance to CO_2 and water contamination, and small surface areas.[5] They are expensive, and the steric hindrance of reactants to the active site due to lower pore size is also a challenge.[6] Therefore, the synthesis or utilization of customized catalysts with better stability, activity, and selectivity is one of the things that the biodiesel production sector requests. The catalyst stability, activity, and selectivity rely on the nature of catalytic precursors and synthesis methods.[1] The strength, concentration, and dispersion of the active sites including the catalyst texture also matter.[7] So, to produce a catalyst with the desired properties, attention must be paid to the catalyst synthesis method and precursor selection.

Received: October 16, 2023
Revised: December 4, 2023
Accepted: December 11, 2023
Published: January 2, 2024

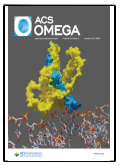

Among heterogeneous catalysts, alkali catalysts provide the highest transesterification rate.[8] Alkali catalysts containing metallic carbonates and oxides have recently gained interest, and they can be made using biological and chemical precursors.[9,10] The metallic carbonates are usually K_2CO_3, Na_2CO_3, $CaCO_3$, and $K_2Ca(CO_3)_2$. They have a strong alkali nature.[1] If the carbonates are transformed into oxides, the alkali strength will be better. The conversion of individual carbonates into oxides usually requires a high thermal energy. However, it can be decreased by employing precursors containing a mixture of carbonates and carbonate composites with modifying agents.[11] Lignocellulosic biomasses (LBs) are among the precursors that are renewable, relatively cheap, and environmentally friendly. Their calcination yields ash with mixed metallic carbonates and other compounds.[9,10] Thermal processing of LBs and their blend with chemical precursors also provides catalysts having blended oxides whose performance and stability are usually better than single oxides.[1] However, alkali catalysts are only efficient for transesterification of feedstocks having low free fatty acids because of the soap formation reaction.[3] Bifunctional catalysts can handle this problem by undergoing simultaneous transesterification and esterification of feedstocks having a high FFA content. Incorporating amphoteric oxides into alkali compounds derived from low-cost materials can provide bifunctional catalysts that can be used to valorize a range of feedstocks into biodiesel.[12,13] An amphoteric metal oxide that is usually employed as a Lewis acid site is ZrO_2.[14,15] The catalytically active polymorph of ZrO_2, tetragonal ZrO_2, is unstable unless it is integrated with other materials. This can be made possible via ZrO_2 supporting and blending.[15,16] Supporting ZrO_2 and other metallic oxides on materials such as silica-rich LB ash also reduces active site leaching due to the formation of metallic silicate.[17] The method of catalyst preparation (for example, mechanical mixing vs in situ titration,[18] coprecipitation, precipitation, and sol−gel method[19]) also influences the catalyst's physicochemical properties and stability.

The most popular method for obtaining the catalyst's active components involves calcining precursors in a limited supply of air. During the calcination process, combustion also occurs. Thus, the combustion performance of precursors and catalyst composite materials (CCMs) plays a crucial role in establishing the catalyst's physicochemical properties.[20] For instance, the ashes produced when the more thermally reactive component in LBs is oxidized may prevent air from penetrating and cause the char produced by the less reactive component not to oxidize.[21] This in return slows the decomposition of organic and inorganic compounds into more catalytically active components.[1] The combustion performance of biomasses can be tuned by techniques such as biomass blending[22] and chemical modification.[23] With this scenario, it may be possible to synthesize catalysts that have more activity and resistance to deactivation from a blend of LBs and chemicals.[1] Thermal analyses, including thermogravimetric and differential thermal analysis techniques, can be employed to understand the combustion mechanism of biomasses and their derivatives.[21]

Coffee and *Eragrostis tef* (teff) are abundant crops in Ethiopia. Their processing introduces byproducts called coffee husk (CH) and teff straw (TS) to the environment. CH ash is rich in alkali metals,[9] whereas TS ash is rich in silica.[24] TS also contains alkali metals such as K and Ca compounds in a small amount. In this study, chars were made from CH and CH blends with TS (CH−TS) as catalyst active site sources and support. The combustion behavior of CH, TS, and CH−TS was investigated. The chars obtained from the calcination of CH and CH−TS were modified with KNO_3 for alkali catalyst synthesis. Bifunctional catalysts containing ZrO_2 as a Lewis acid site and alkali sites from CH ash were also synthesized via precipitation of $Zr(NO_3)_4{\cdot}H_2O$ solution followed by impregnation and direct impregnation of $Zr(NO_3)_4{\cdot}H_2O$ onto CH char by using an ultrasonic bath. The comparative performance and reusability test of the synthesized catalysts were performed by crude WFO transesterification. The catalysts' response to the transesterification of water-blended WFO was also investigated. The scientific community potentially gets new knowledge from this study toward the preparation of customized catalysts for biodiesel synthesis by integrating biological (LBs) and chemical precursors.

MATERIALS AND METHODS

Materials. Coffee husk (CH) and teff straw (TS) were collected from Dilla and around the Addis Ababa region, Ethiopia, respectively. Potassium nitrate (KNO_3 (98%)) and zirconium nitrate ($ZrO(NO_3)_2{\cdot}H_2O$ (99%)) were bought from local chemical retailers in Addis Ababa, Ethiopia.

Material Preparation and Characterization. The waste frying oil (WFO) that was obtained from local sellers of fried fish was filtered, dried, and stored in a sealed container. Using ISO 660:2020 and AOCS 920.160 standard procedures, the WFO ready for the transesterification acid and saponification values were determined, respectively. Using calculations based on the peak area for protons in various environments, the composition of the oil was determined by ^{1}H NMR spectroscopy analysis (eqS 1−4).[25]

$$\mathrm{Ln}(\%) = 100\left(\frac{B}{A+B}\right) \quad (1)$$

$$\mathrm{L}(\%) = 100\left[\frac{E}{D}\text{-}2\left(\frac{B}{A+B}\right)\right] \quad (2)$$

$$\mathrm{O}(\%) = 100\left[\frac{C}{2D}\text{-}\frac{E}{D} + \left(\frac{B}{A+B}\right)\right] \quad (3)$$

$$\mathrm{S}(\%) = 100\left[1\text{-}\frac{C}{2D}\right] \quad (4)$$

In these formulas, Ln is linolenic, L is linoleic, O is oleic, and S is the saturated acids of the triglyceride. A represents the methyl hydrogen atom of saturated oleic and linoleic acyl groups; B represents methyl hydrogen atoms of linolenic acyl groups; C represents methylenic hydrogen atoms in position α in relation to one double bond (also named allylic protons); D represents methylenic hydrogen atoms in position α in relation to a carboxyl group; and E represents methylenic hydrogen atoms in α position with respect to two double bonds, also named bis-allylic protons.

The CH and TS moisture content was reduced via sun drying followed by oven drying and then ground with a coffee grinder (M.M2112). A CH and TS blend (CH−TS) was also prepared by homogenizing the CH and TS powders using the coffee grinder. The blending was aimed to get a complex of silica and alkali metal compounds during catalyst preparation. TS ash is rich in silica,[24] whereas CH ash is rich in alkali metal compounds as per our previous study.[9] Silica and alkali metal compounds react during calcination to generate metallic

https://doi.org/10.1021/acsomega.3c08108
ACS Omega 2024, 9, 2815−2829

silicates, which improve the chemical stability of the catalyst.[17] Our preliminary experiments showed that the formation of metallic silicates was successful when utilizing char derived from CH−TS with a CH to TS blending weight ratio of 4 to 1 during catalyst preparation (explained in the Alkali Catalyst Preparation section). The CH proximate analysis values were taken from our previous study.[9] The TS and CH−TS proximate analyses were performed according to the ASTM standard methods. These are E1756-08 for the moisture content (MC), E1755-01 for the ash content (AC), and E872-82 for the volatile matter content (VM). The fixed carbon (FC) content was calculated using eq 5:

$$\mathrm{FC(wt\%)} = \mathrm{100\text{-}MC\text{-}AC\text{-}VM} \quad (5)$$

Alkali Catalyst Preparation. The method from our previous research was adopted for the alkali catalyst synthesis procedure with slight modifications.[9] The CH and CH−TS powders were calcined at 600 °C for 2 h to obtain chars that were designated as A/C and mA/C, respectively. A 24 g portion of A/C and 24 g of mA/C were separately impregnated (incipient wetness impregnation) with 3.06 g of KNO_3 in an ultrasonic bath and then dried at 110 °C for 4 h to get catalyst composite materials (CCMs). The dried CCMs were labeled as CCM-45 (i.e., KNO_3/(A/C)) and CCM-Mix (i.e., KNO_3/(mA/C)). The sample CCM-45 was calcined at 600 °C for 3 h to obtain the alkali catalyst (i.e., C-45). Similarly, the other alkali catalyst (i.e., C-Mix) was obtained by calcination of CCM-Mix at 600 °C for 2.5 h and then at 700 °C for 0.5 h in a limited air. The label "C" in C-45 and C-Mix stands for catalyst, whereas "45" and "Mix" stand for the amount of KNO_3 in wt %[9] and mixture of coffee husk and TS char, respectively.

Bifunctional Catalyst Preparation. To examine the impact of the catalyst synthesis effect, two bifunctional catalysts were synthesized. The first one was $ZrO(NO_3)_2 \cdot H_2O$ (ZN) precipitation using a titrant extracted from CH ash dissolution in distilled water followed by incipient impregnation onto A/C. The CH ash for titrant extraction was prepared by calcination of the dry CH at 800 °C for 2 h followed by open-air burning for an hour. The titrant solution was then dropped at 1.5 mL/min into a ZN solution in a beaker (3.06 g ZN in 35 mL distilled water) until a viscous precipitate was obtained. The precipitate was then impregnated onto the A/C at 35 °C for 1 h using an ultrasonic bath. The catalyst composite material was then dried in a circulating air oven at 110 °C for 4 h and calcined for 3 h at 600 °C to get the catalyst (Bic-PP). The other bifunctional catalyst (Bic-Dm) was made in a similar condition to the alkali catalyst (C-45) with the exception that ZN was impregnated onto A/C. Because A/C is alkaline in nature, precipitation takes place simultaneously during the ZN impregnation process.

Catalyst Characterization. The crystalline phases in each catalyst were determined using an X-ray diffractometer (Shimadzu XRD-7000, Japan) that used Cu Kα radiation (=0.15406 nm) and operated at 40 kV and 44 mA. With a step size of 0.02° and a scanning speed of 10°/min, the 2θ values had a range of 5 to 80°. The surface area of catalysts was estimated using the Brunauer−Emmett−Teller (BET) method using a surface area analyzer (Horiba Instruments, Inc. SA-9600 series, USA). The samples were oven-dried overnight at 110 °C and degassed for 3 h at 150 °C before the experiment for BET analysis. The catalysts' surface morphology was scanned using a scanning electron microscope (JCM-6000Plus, Germany). A Thermo Scientific Nicolet IiS50 ABX smart iTX Fourier transform infrared spectrometer was used in conjunction with the ATR technique to identify the vibration mode of functional groups in the catalysts. In the range of 400 to 4000 cm^{-1}, 32 scans with 16 cm^{-1} resolution were made.

The catalysts' pH was measured by taking each catalyst filtrate (extracted from a dissolution of 0.5 g of catalyst in 10 mL distilled water for 30 min) and measuring their pH using a digital pH meter (Hanna Instruments pH meter, HI 83141).[26] The Hammett indicator method, as described in our previous work,[9] was used to measure the strength of the alkali sites on the C-45 and Bic-Dm catalysts. The total alkalinity of the catalysts was assessed using the phenolphthalein Hammett indicator and 0.01 M benzoic acid in toluene as a titer. The first 30 min was spent stirring a suspension of 0.15 g of catalysts in a solution of phenolphthalein in toluene (2 mL, 0.1 mg/mL). Finally, the suspension was titrated using a 0.01 M solution of benzoic acid in toluene. The titration end point was seen as when the mixture turned from pink to colorless. The leachable alkalinity determination was started by stirring 0.5 g of the catalyst in 50 mL of distilled water for 1 h at room temperature. Then, the solution was filtered to get a clean filtrate free of catalyst particles. The clear filtrate was mixed with a methanol solution of phenolphthalein (5 mL, 0.1 mg/mL) and titrated using a toluene solution of benzoic acid (0.01 M).[27]

Thermal Analysis. By utilizing methods previously stated,[28,29] the combustion performance of CH, TS, CH−TS, and catalyst composite materials (CCMs) was examined using thermal gravimetric analysis (TGA) results. Thermal gravimetric analysis (TGA) was conducted by employing a Shimadzu DTG-60H (Japan) instrument. The DTG curve was generated from TG vs time (t) data. The TG-DTG curves were used to estimate the necessary values for the combustion indices such as indices of comprehensive combustion (S), burnout (D_f), ignition (D_i), and combustion stability (H_f) value calculation. The sample size during each thermal analysis was 10 ± 0.0001 mg in alumina crucibles. The temperature ranged between room temperature and 800 °C. The thermal decomposition took place with a heating rate of 20 °C/min in the absence of external feed flow rate of air with the TG system. Thermograms were plotted using data from duplicate trials and averaged.

Catalyst Performance Evaluation. The effect of temperature (35 to 75 °C with 10 °C increment), catalyst loading (1 to 9 wt % with 2 wt % increment), methanol to WFO molar ratio (9:1 to 21:1 molar ratio with 3:1 increment), and reaction time (20 to 120 min with 20 min increment) at a fixed mixing rate of 600 rpm on the performance of the catalysts for transesterification of WFO were investigated. Based on our earlier[9] and preliminary analysis, the range of the parameter values was established. After the transesterification reaction completion, the catalyst was separated via centrifugation at 1200 rpm for 20 min, and then the WFO glycerol mixture was aged overnight to aid in glycerol separation. The residual contaminants in the WFOME were removed by washing with hot distilled water.[9] The washed WFOME was then dried at 110 °C for 4 h and stored in a sealed container for further analysis. The WFO and WFOME weights were related using eq 6 to calculate the WFOME yield.[30] Further, to show the potentiality of the catalysts, their turnover frequency (TOF) was calculated using eq 7.[31] During TOF calculation, the total alkalinity of the catalysts was considered, and the molecular

https://doi.org/10.1021/acsomega.3c08108
ACS Omega 2024, 9, 2815−2829

weight (MW) of the WFOME was assumed to be one-third that of the WFO.

$$Y(\text{wt\%}) = \frac{\text{WFOME weight}}{\text{WFO weight}} \times 100 \quad (6)$$

where Y represents the yield of the WFOME (wt %)

$$\text{TOF} = \frac{\text{moles WFOME produced(mmol)}}{\text{catalyst's alkalinity(mmol)} \times \text{time(h)}} \quad (7)$$

Catalyst Reusability Test. The catalyst was recovered for a reusability test via methanol followed by acetone washing of the spent catalyst. The reusability test was also performed after regeneration using the recalcination of recovered catalysts at 600 °C for 2 h for all catalysts except for the recovered C-Mix. The recovered C-Mix was regenerated via calcination at 600 °C for 1 h followed by 700 or 0.5 h. The reusability test was performed using 15:1 methanol to WFO molar ratio at a reaction temperature 65 °C for 1 h reaction time with catalyst loading of 5 wt % for the alkali and 7 wt % for the bifunctional catalysts.

RESULTS AND DISCUSSION

WFO Characteristics. The WFO had an acid value of 2.52 mg KOH/g oil (i.e., 1.26% of FFA). It is close to the waste cooking oil FFA content (1.27%) reported by Al-Hamamre et al.[32] The saponification value of WFO was found to be 197 mg KOH/g. The fatty acid composition of the WFO was calculated based on integral areas of the the WFO ^{1}H NMR spectrum (Figure 1) using eqs 1−4. It was revealed that WFO

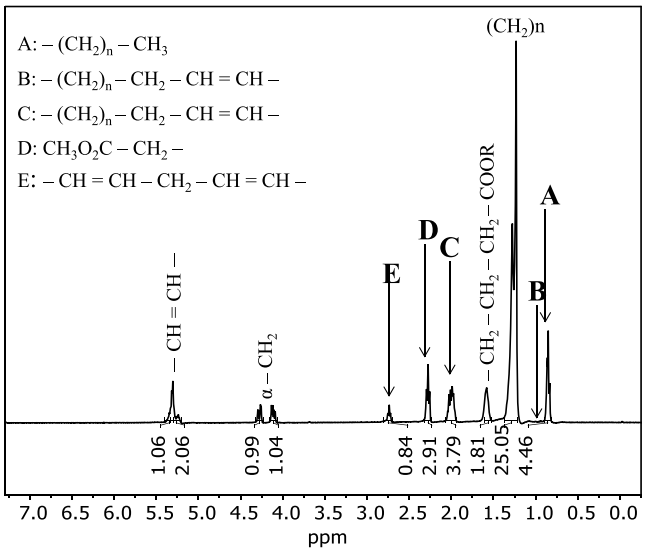

Figure 1. ^{1}H NMR spectra of the WFO.

comprises monounsaturated, polyunsaturated, and saturated fatty acids (Table 1). The amount of linoleic and oleic acid was determined to be 28.87 and 36.65%, respectively. The WFO contains about 34.88% saturated fatty acids. In Ethiopia, it is common to fry foods in palm oil, and it may be the reason that the WFO fatty acid profile contained high concentrations of unsaturated fatty acids. The lower unsaturated fatty acid composition than palm oil (CPO) (Table 1) may be due to blending with other oils such as sunflower oil. Compositional changes during frying (for example, UnFO vs UFO (Table 1)) may also be the reason.[33] The WFO in this study is suspected

Table 1. Fatty Acid Composition of WFO and Comparison with Those of Earlier Studies[a]

fatty acid	structure ($C_{X:Y}$)[a]	composition (%)				
		this study	RSO25	CPO35	UnFO33	UFO33
linoleic acid	18:2	28.87	39.86	10.2	57.36	53.86
linolenic acid	18:3		13.17	0.3	6.25	3.02
oleic acid	18:1	36.25	27.06	39.8	23.0	28.87
saturated acid	X:0	34.88	19.91	47.8	13.45	14.25

[a]X and Y are the numbers of carbon and a double bond in the fatty acids, respectively. UnFO: unused frying oil, UFO: used frying oil, CPO: crude palm oil, and RSO: rubber seed oil.

of offering biodiesel with poor cold flow characteristics due to the higher percentage of saturated fatty acids.[34] However, the presence of a higher saturated fatty acid composition is good for the oxidation stability of biodiesel.[1] Therefore, to obtain biodiesel with better cold flow properties and oxidation stability, blending the WFO with feedstocks having higher unsaturated fatty acid compositions like UFO, RSO (Table 1), and others may be recommended.[1]

Proximate Analysis of CH, TS, and CH−TS. The proximate analysis of the LB samples is presented in Table 2. The moisture content (less than 10 wt %) of the biomasses

Table 2. Proximate Analysis of the Biomasses for Catalyst Synthesis

lignocellulosic biomass	MC (wt %)	AC (wt %)	VM (wt %)	FC (wt %)
CH	5	5.26	70.02	22.32
TS	6	5.24	75.05	13.71
CH−TS	5.02	5.43	72.05	17.50

is less than most undried biomasses and is convenient for combustion. The primary component in the biomasses is the volatile matter (70.02 to 75.05 wt %), which can be eliminated during the pyrolysis stage of the calcination and serves as a fuel that promotes biomass burning during the preparation of the chars (A/C and mA/C).[36] Biomass blending resulted in a catalyst precursor (CH−TS) having more volatile matter content than CH, which contributes to the better combustion performance of CH−TS than CH.[37] The ash content of the CH, TS, and CH−TS is close to the ash content of the pineapple leaves (6 wt %) and higher than *cupuacu* seeds (2.6 wt %) that were previously studied as a precursor for heterogeneous ash catalyst preparation.[38] Even though their low ash content yields a low amount of catalyst, it will make them convenient for energy production in combustors.[36] Because of its larger fixed carbon content, CH is predicted to have a higher heating value than TS and CH−TS.[39]

Thermal and Combustion Performance Analysis. According to the TG, DTG, and DTA thermograms of CH, TS, and CH−TS (Figure 2a−c), the first step is moisture removal, which contributed 5, 6.8, and 4.8 wt % of the mass loss, respectively. The loss may also comprise a small quantity of light volatile matters. For CH, the second stage might result from the hemicellulose's xylan backbone side chain cleavage,[40] which is demonstrated in the CH's DTG curve at a peak temperature of 222 °C. The CH−TS experienced this peak at

https://doi.org/10.1021/acsomega.3c08108
ACS Omega 2024, 9, 2815−2829

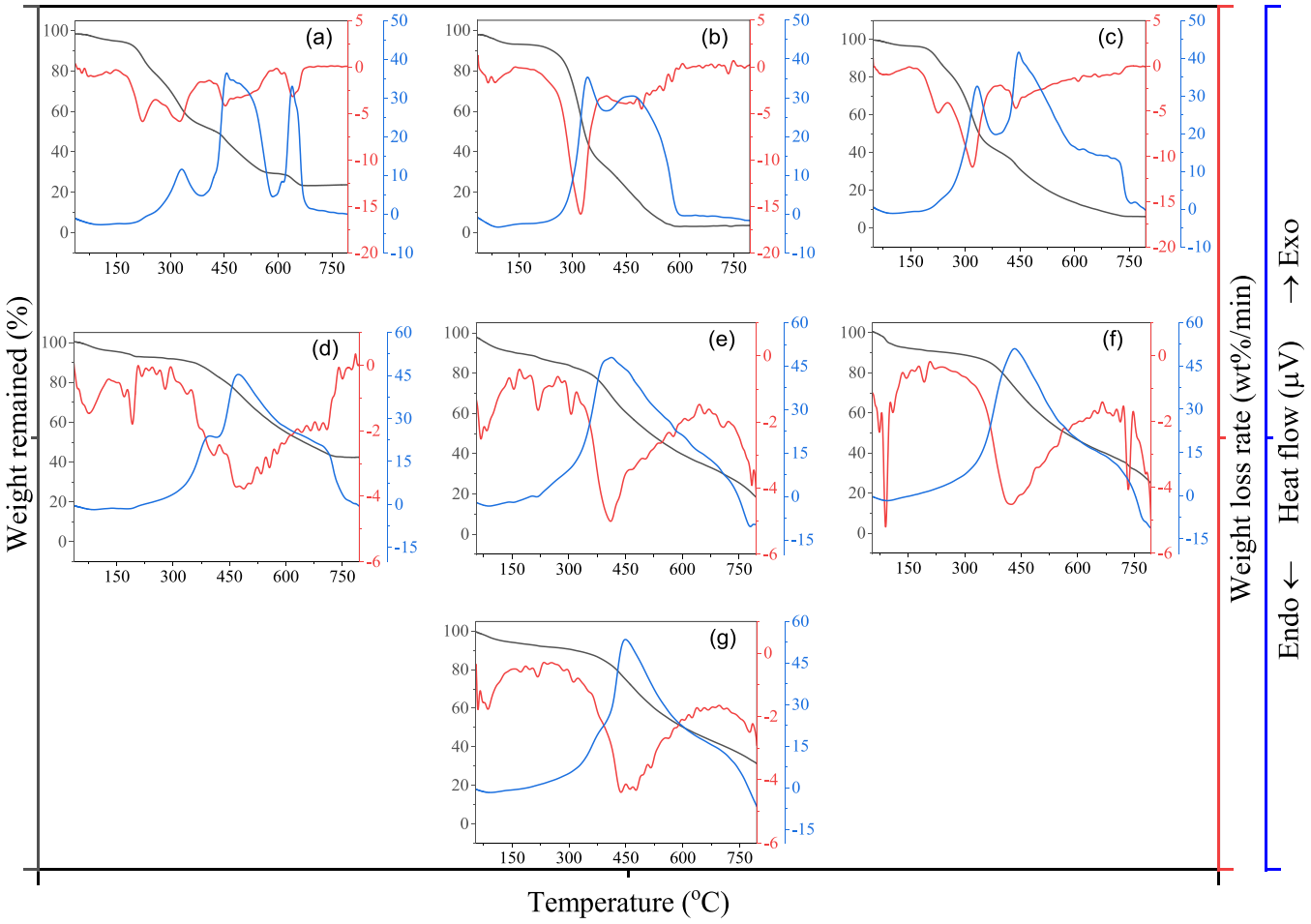

Figure 2. TG-DTG-DTA curves of (a) CH, (b) TS, (c) CH−TS, (d) CCM-45, (e) CCM-Mix, (f) CCM-Dm, and (g) CCM-PP under air atmospheres.

226 °C, whereas the TS did not. The cellulose−hemicellulose decomposition peaks for TS were merged and appeared at a peak temperature of 323 °C with a maximum weight loss rate of 15.89 wt %/min. Because of the degradation of predominantly cellulose and partially hemicellulose as well as lignin, a third DTG peak for CH was observed around 326 °C. The DTG peak in the 385−585 °C range shows that the CH degradation proceeded, along with residual lignin degradation and previously produced char burning.[41] The DTG peak for the CH at 640 °C is due to residual char burning and probably inorganic component volatilization.[42] This peak most likely occurred as a result of the previously developed ash's nonporous character for air transfer.[21] The absence of the residual carbon combustion peak, which appeared during the CH calcination, is most probably due to the porous nature of previously produced ash and char from TS and CH−TS decomposition for air transport. This suggests that TS mixing enhanced the CH's combustion performance by most likely altering the ash's composition and increasing the volatile matter content.[21,43] Therefore, according to the thermal analysis, 600 °C is adequate for the efficient breakdown of CH, TS, and CH−TS while still leaving some char for active site precursor's (KNO_3 and ZN) impregnation during the preparation of the catalysts. From the DTA curves, the maximum heat flows for CH, TS, and CH−TS decomposition were found to be 37, 31, and 42 μV at 457, 465, and 447 °C, respectively. The higher heat flow at the main burning stage is an indicator of CH−TS's better burning property.[42]

The TG-DTG-DTA curves for catalyst composite materials (CCMs) are presented in Figure 2d−g. In the range of 30 to 155 °C, moisture removal is the initial stage for all TG-DTG curves of the CCMs and is then followed by the evacuation of volatile matters. The difference in shape and temperature range of the CCMs DTG profiles in the main combustion stage shows the differences in the CCMs' heterogeneity. The heterogeneity may arise from compositional differences and nonuniformity in the dispersion of components. The burnout temperature is 651 °C for CCM-45 and greater than 800 °C for the other CCMs. These burnout temperatures are greater than most biomass-derived chars and close to coal.[44] Therefore, the combustion performance of the CCMs is poor compared to LBs chars that were used as a building block to make them.

Based on the corresponding TG-DTG graphs (Figure 2), temperatures for maximum weight loss rate (T_p), maximum weight loss rate (DTG_{max}), burnout temperature (T_b), and ignition temperature (T_i) were estimated (Table 2) according to the method reported by Liu et al.[29] The other values that were determined from the TG-DTG curves are the maximum peak time (t_p), burnout time (t_b), and the time range of DTG/DTG_{max} = 0.5 ($\Delta t_{1/2}$). In contrast to its inverse relationship with peak temperature, sample combustion reactivity is directly related to the maximum rate of weight loss.[22] In this regard, TS

https://doi.org/10.1021/acsomega.3c08108
ACS Omega 2024, 9, 2815−2829

Table 3. Combustion Characteristic Parameters of Coffee Husk, Teff Straw, Blend of Husk and Straw, and Composite Materials at 20 °C/min Heating Rate[a]

property↓ materials	T_i (°C)	T_b (°C)	T_p (°C)	DTG_{max} (wt %/min)	t_i (min)	t_b (min)	t_p (min)	DTG_{av} (wt %/min)	$\Delta t_{1/2}$ (min)	D_i (wt % min^{-3})	D_f *10^4 (wt % min^{-4})	S *10^7 (min^{-2} $°C^{-3}$)	H_f (wt % min^{-1} $°C^3$)
CH	188	484	326	5.86	8.10	22.94	14.52	3.59	8.77	0.050	20.00	12.3	291
TS	272	397	322	15.81	12.34	18.60	14.84	8.64	13.01	0.086	66.36	46.51	132
CH−TS	249	415	320	11.18	10.55	18.81	14.06	5.54	11.76	0.075	35.95	24.07	241
CCM-45	329	651	487	3.78	15.24	31.36	23.15	3.02	17.25	0.011	3.02	1.62	849
CCM-Mix	283	nd	411	5.03	12.87	nd	19.27	nd	16.92	0.020	nd	nd	nd
CCM-Dm	318	nd	424	4.52	14.18	nd	19.48	nd	16.78	0.016	nd	nd	nd
CCM-PP	331	nd	437	4.43	14.65	nd	19.95	nd	17.55	0.015	nd	nd	nd

[a]nd: not determined.

attained the maximum weight loss rate (15.81 wt %/min) followed by CH−TS (11.18 wt %/min); these values are by far larger than the CH's (5.6 wt %/min) with insignificant peak temperature differences. The higher temperature for the maximum weight loss rate of the CH is an indicator of CH's higher fixed carbon content (Table 2). Teff straw has a higher rate of weight loss because it contains the highest amount of volatile matter (Table 2). By having lower burnout temperature (T_b) and burnout time (t_b) values than CH, CH−TS exhibited a higher combustion performance. This implies that the char from CH−TS (mA/C) for KNO_3 impregnation can be obtained with a shorter calcination time than the char from CH (A/C). Additionally, for identical combustion conditions of CH and CH−TS, the unburned carbon loss will be smaller for CH−TS if used as a fuel.[22] Therefore, via CH blending with TS, CH−TS with better thermal reactivity than CH was obtained.

The combustion indices (Table 3) were also employed to compare the combustion performance. They were determined using formulas taken elsewhere.[20] The indices were burnout (D_f), comprehensive combustion (S), ignition (D_i), and combustion stability (H_f). Having the highest D_i, D_f, and S and lower H_f values implies that the material has the best combustion performance. In this regard, the TS demonstrated excellent combustion performance. The lowest combustion performance belongs to CH. However, by the 20 wt % TS addition into CH, the CH−TS with a combustion performance between TS and CH was obtained. This is most probably because of the TS addition; the CH−TS acquired a higher volatile matter concentration than CH, which contributes to the improved combustion performance.[37]

The combustion indices' values of the CCMs are also presented in Table 3. Because of the elimination of volatile components, the CCMs displayed lower thermal reactivity when compared to the LBs.[42] The higher D_i, D_f, and S and lower H_f values are for CCM-Mix, which indicate its higher thermal reactivity. The order of thermal reactivity is CCM-Mix > CCM-Dm > CCM-PP > CCM-45. Generally, based on the thermal reactivity, CCM catalysts with different physicochemical properties were obtained. For example, the higher thermal reactivity may be the reason for obtaining C-Mix catalyst from CCM-Mix calcination with K_2O (Figure 6) and negligible unburned char content and light green color from visual observation (Figure 3).[45] The composition of the CCM and ash derived from it may play a role in affecting the thermal reactivity; for example, for small-size samples, ash rich in alkali compounds plays a catalytic role for char combustion, but for large-size samples, it has physical effects.[21] The TG-DTG-DTA (Figure 2d−g) curves show the heterogeneity in the combustion of the CCMs. Therefore, attenuation in thermal reactivity for less reactive components is likely due to an oxidation delay caused by the reduced air transfer rate because of ash formed from completely burnt more reactive components.[21]

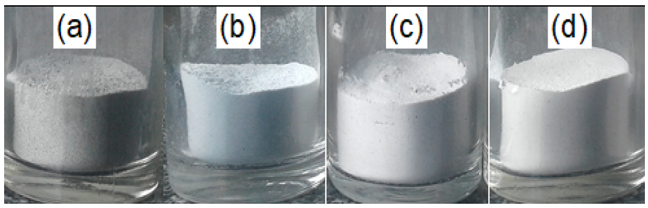

Figure 3. Photograph image of catalysts (a) C-45, (b) C-Mix, (c) Bic-Dm, and (d) Bic-PP visual observation

Catalysts' Visual Observation. The appearance of the catalysts is depicted in Figure 3. These samples came in a variety of tones, from dark gray (Figure 3a) and light green (Figure 3b) to light gray (Figure 3c,d). The dark color of C-45 was probably due to the unburned char residue, which indicates incomplete combustion of the CCM-45 contents.[46] This is probably due to the lower thermal reactivity of the CCM-45 sample (Table 3). Additionally, a reduced global thermal reactivity for a larger sample size during the C-45 synthesis may also contribute. During the calcination of CCM-45, ash may rapidly be formed and increase resistance for air transport, which then reduces char oxidation at the bottom in a crucible.[21] The C-Mix catalyst was obtained as a light bright green powder, indicating the reaction of components such as silica from TS ash with potassium and another trace amount of alkali metals to form metallic silicate. For a silica-supported chromium complex catalyst, the same phenomenon was also noted as reported by Monoi and Sasaki.[47] Rice straw ash changed from dark gray (450 °C) to light gray (600 °C) and then to light purple at 815 and 1000 °C.[45] The color change observed during the calcination process was justified by the reaction of the ash components.[45]

Catalysts' pH and Alkalinity. The pH of catalysts was determined to be 11.93 (C-45), 12.94 (C-Mix), 11.17 (Bic-Dm), and 11.23 (Bic-PP) (Figure 4). The pH of the bare CH ash catalyst from the calcination of A/C at 600 °C for 3 h without KNO_3 impregnation was measured to be 11.4. This pH value was close to lignocellulosic biomass ashes derived from waste *Sesamum indicum* plant (11.3)[26] and Karanja seed shell (11.46).[48] However, these pH values are lower than the pH of alkali catalysts in this study, which may be due to an increase in K content via the KNO_3 impregnation.[9] Because CCM-Mix has better combustion performance than CCM-45 (Table 3), C-Mix may acquire a larger density of basic

https://doi.org/10.1021/acsomega.3c08108
ACS Omega 2024, 9, 2815−2829

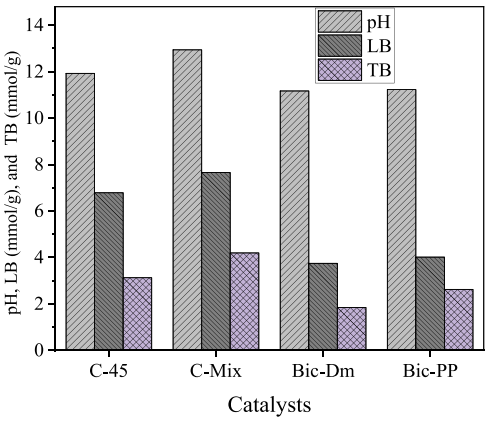

Figure 4. Synthesized catalysts pH, leachable alkalinity (LB), and total alkalinity (TB) values.

components due to the absence of unburned char. This phenomenon was confirmed during the visual observation of the catalysts and thermal analysis of CCMs. The decreased pH of the Bic-Dm and Bic-PP catalysts compared to the alkali catalysts is due to the amphoteric nature of the impregnated ZrO_2.[15] This evidenced that the nature of the heterogeneous catalysts is tunable to the required acidic or basic strength. In addition to the ZrO_2 impregnation, the catalyst pH was affected by the biomass blending. The reason behind the high pH of all catalysts was due to the catalyst potassium and other alkali compound contents, as explained during the XRD and FTIR analysis (Figures 5 and 6).

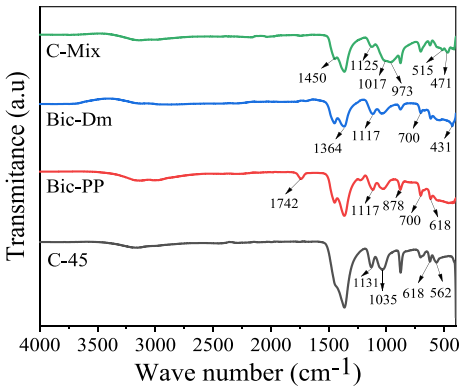

Figure 5. FTIR spectra of the synthesized alkali and bifunctional catalysts.

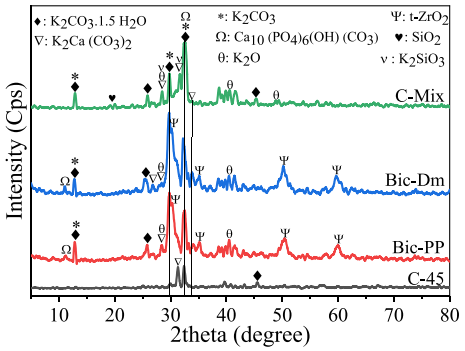

Figure 6. XRD profiles of the synthesized alkali and bifunctional catalysts.

The estimated leachable alkalinity values of C-45, C-Mix, Bic-Dm, and Bic-PP catalysts were found to be 7.79, 8.66, 4.75, and 5.02 mmol/g, respectively. The respective values for the total alkalinity were 3.13, 4.20, 1.85, and 2.63 mmol/g (Figure 4). The C-Mix catalyst has the highest leachable and total alkalinity values. The highest alkalinity of the C-Mix catalyst was due to high quantities of K, C, and O in the form of carbonate of K and other metals.[49] Alkali silicates, mainly potassium silicate as indicated in the XRD analysis of C-Mix (Figure 6), may also be the reason for the strong alkalinity.[8] The lower alkalinity of C-45 compared to C-Mix may be due to the presence of unburned char, which reduces the relative composition of metallic carbonates and oxides. The lower leachable and total alkalinities of the bifunctional catalysts (Bic-Dm and Bi-PP) are probably due to the presence of the amphoteric t-ZrO_2[15] and lower concentration of K-containing compounds.[49] In all cases, the total alkalinity is lower than the leachable alkalinity (LB) maybe because of the catalysts' very low surface area (<3 m^2/g). Water washing makes it possible for the alkali sites inside the structure to be leached, whereas a catalyst with a low surface area conceals those sites and prevents toluene titration.[9,27] The presence of metal oxides and carbonates in all of the present catalysts was supported by the XRD analysis (Figure 6). According to Sharma et al.,[11] chemically activated wood ash (calcined at 800 °C) loaded with K_2CO_3 and $CaCO_3$ produced 12.7 and 8.8 mmol/g of soluble alkalinity, respectively, which are greater than catalysts in this work. In another study, it was reported that the estimated leachable alkalinity values of *Musa Champa* peel, stem, and rhizome ash catalysts were found to be 7.13, 4.77, and 5.21 mmol/g, respectively, which are lower than the alkalinity of alkali catalysts and close to bifunctional catalysts in this study.[49]

FTIR Analysis of Catalysts. All catalysts have similar FTIR spectra, except for a few differences. The C-Mix showed bands at 471 and 973 cm^{-1} that belong to the Si−O stretching and 1017 cm^{-1} asymmetric stretching for Si−O−Si bond vibrations.[50] These bands are most probably due to the presence of potassium silicate that is potentially responsible for the light green color of the C-Mix catalyst.[51] The characteristic band vibration at 515 is also evidence of the presence of a Si−O bond.[52] The PO_4^{3-} bending vibration band at 1131 cm^{-1} for the C-45 that shifted to 1117 cm^{-1} with increased intensity (may be due to increased polarity) for Bic-Dm and Bic-PP is an indicator of the incorporation of t-ZrO_2 in their structure. For all catalysts, the bands represented by 1035 cm^{-1} belong to P−O symmetric stretching vibrations in carbonated hydroxyapatite.[53] The catalysts also revealed the carbonate compounds' existence in their structure via bands at 145 and 1364 cm^{-1} that belong to the C−O stretching and bending vibrations, respectively.[9] The bands at 562, 618, and 700 cm^{-1} are for M−O vibrational stretching where M represents metals, mainly K.[26,54] According to the results of the FTIR study, the active sites for transesterification are found to contain metallic carbonates and oxides.

XRD of Catalysts. The qualitative information on crystalline phases in the catalysts was extracted from XRD diffraction patterns (Figure 6) analysis. Our earlier catalyst XRD analysis[9] served as the foundation for the peak assignment in this work. Additionally, JCPDS cards with the numbers 11-0655 for $K_2CO_3{\cdot}1.5H_2O$, 21-1287 for $K_2Ca(CO_3)_2$, 71-1466 for K_2CO_3, and 17-0923 for tetragonal zirconia (t-ZrO2) were used. Further, the literature that

https://doi.org/10.1021/acsomega.3c08108
ACS Omega 2024, 9, 2815−2829

investigated acai seed ash[54] and waste *Musa paradisiaca* plant[55] ash solid alkali catalysts was also considered to identify the presence of K_2O crystals. Supported zirconia bifunctional catalysts were also considered.[56,57] The main crystals found in the alkali catalysts are $K_2Ca(CO_3)_2$, K_2CO_3, and $K_2CO_3 \cdot 1.5H_2O$. These components are common in ash catalysts derived from lignocellulosic biomasses such as cocoa pod husk−plantain peel blend,[58] waste *Musa paradisiaca* plant,[55] and wood ash.[11] Based on the XRD patterns (Figure 6), the relative composition of $K_2Ca(CO_3)_2$ seems higher in the C-45 catalyst when compared to the others. The XRD peaks at 28.5, 40.5, and 48.4° indicated the presence of K_2O. The presence of $K_2Ca(CO_3)_2$, K_2CO_3, and K_2O contributed to the alkalinity strength of the catalysts (Figure 4). In addition to these crystals, the bifunctional catalysts included the Lewis acid site source tetragonal zirconia (t-ZrO_2) crystal in their structure. Because it is the catalytically active form, obtaining only the tetragonal (t-ZrO_2) than the monoclinic (m-ZrO_2) and cubic polymorphs of ZrO_2 is advantageous.[59] However, obtaining a catalyst with a mixture of t-ZrO_2 and m-ZrO_2 is the most common one.[56,57] A catalyst with only the t-ZrO_2 phase is rarely reported.[15,59] The t-ZrO_2 phase in the bifunctional catalysts was successfully obtained for this study. Characteristic peaks were observed at 30, 50, and 60°, which reveal the presence of t-ZrO_2 crystals in Bic-Dm and Bi-PP structures. Thus, the bifunctional nature of Bic-Dm and Bic-PP was due to the presence of alkali metal carbonates, K_2O, and the amphoteric t-ZrO_2 phases. This enables the bifunctional catalysts to undertake simultaneous esterification and transesterification of WFO free fatty acid and triglycerides. A K_2SiO_3 crystal in C-Mix may also contribute to peaks at 28.53 and 31.7°. This crystal was investigated as an alkali site in a catalyst for biodiesel production and offered high alkalinity.[8]

SEM Analysis of Catalysts. Scanning electron microscopy (SEM) was used to examine the surface morphology and revealed the presence of agglomerated and large particles for all of the catalysts (Figure 7). The SEM image in Figure 7 for C-45 demonstrated a mixture of particles having flake and rod morphologies in a variety of sizes and shapes. This morphology might be due to the presence of mixed carbonates and a relatively large $K_2Ca(CO_3)_2$ content, as explained during XRD analysis. A fairly similar flake and rod-like morphology was also reported for the SEM image of potassium−calcium (K−Ca) double carbonate containing materials.[60] The C-Mix catalyst showed a morphology with relatively small-size agglomerates. Contrary to the C-45 catalyst, the $K_2Ca(CO_3)_2$ content of the C-Mix catalyst seems lower, which could account for the smaller agglomerate sizes. For Bic-Dm and Bic-PP catalysts, this behavior was not observed, probably because of the relatively lower concentration of $K_2Ca(CO_3)_2$. The agglomeration in the C-Mix catalyst may be due to the formation of metallic silicates. Some metallic silicates may have lower melting points and a sticky character that can induce agglomeration.[61] This may cause pore blockage and reduce the surface area. The C-Mix morphology was near to the one reported by El-Maghraby et al.[62] for a K_2SiO_3-containing compound induced from catalyst composite calcination at 800 °C. The ash catalyst from the calcination of orange peel[63] in which the dominant phase is K_2CO_3 showed a nearly similar morphology to Bic-Dm and Bic-PP. The slight difference may arise due to composition differences, mainly the presence of t-ZrO_2 in the bifunctional catalysts. The porous nature of the t-ZrO_2-containing catalyst was reported by Fatimah et al.[15] The SEM image analysis shows that the morphology of the heterogeneous catalyst can be tuned based on the CCMs composition and synthesis method.

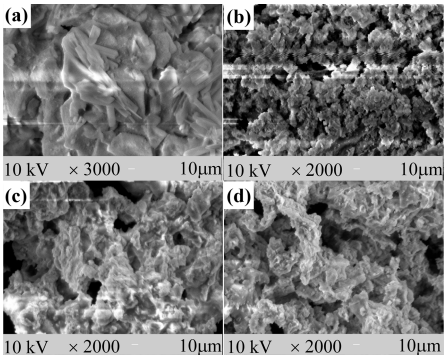

Figure 7. SEM micrographs of (a) C-45, (b) C-Mix, (c) Bic-PP, and (d) Bic-Dm.

BET Surface Area Analysis. The catalyst surface area was measured using the BET method from N_2 adsorption−desorption data and is presented in Table 4. The surface areas are low when compared to most heterogeneous catalysts. However, higher transesterification performance with lower surface area was reported for several heterogeneous catalysts.[32,64,65] Hence, the catalytic performance of heterogeneous catalysts for transesterification reaction strongly depends on active site strength as compared to the surface area (Tables 4 and 5). Further, the present study shows that the surface area of catalysts is a function of the CCM type. The maximum surface area was 2.644 m^2/g for a catalyst from CCM-Dm calcination (Bic-Dm). The larger surface area of Bic-Dm may be related to its porous nature, as demonstrated during the SEM image analysis (Figure 7c). Even though the agglomerate sizes for C-Mix look smaller, the surface area was also smaller (Figure 7b). The result was attributed to the pore blockage via melting of the produced metallic silicates.[61] The formation of metallic silicates is described during FTIR and XRD analysis of the catalysts. The larger agglomerate size is probably the reason for the low BET surface area of the C-45 catalyst (0.776 m^2/g). The degree of crystallinity and amorphous nature that can be demonstrated by the XRD peak intensity and broadness may also potentially contribute to the variation of the BET surface area of the catalysts in this study.[9]

WFOME Characterization Using ^{1}H NMR Spectroscopy. The synthesized WFOME's chemical makeup was identified using ^{1}H NMR. A new signal (not appearing in the WFO's ^{1}H NMR spectrum (Figure 8)) was observed that

Table 4. BET Surface Area of Catalysts Obtained under Different Synthesis Conditions[a]

catalyst	C-45[b]	C-Mix[b]	Bic-Dm[b]	Bic-PP[b]	Li_2CO_3-PHA64	KNO_3/OSA32	CaO/FA65	KNO_3/FA66	ZrO_2/BLA15
surface area (m^2/g)	0.776	0.873	2.644	nd	1.21	1.759	0.701	0.38	56.12

[a]nd: not determined, PHA: peanut husk ash, OSA: oil shale ash, FA: fly ash, and BLA: bamboo leaf ash. [b]This work.

https://doi.org/10.1021/acsomega.3c08108
ACS Omega 2024, 9, 2815−2829

Table 5. Synthesized Catalysts' Performance Comparison with Other Heterogeneous Catalyst for Biodiesel Production[a]

catalyst	calcination conditions (tem. (°C), time (h))		transesterification reaction conditions				BD (wt %)	ref
	for active site[b], support[c]	for CCM calcination	CL (wt %)	MOMR	Rt (h)	RT (°C)		
C-45	(600, 2)[c]	600, 3	5	15:1	1	65	97.07	this work
C-Mix		600, 2.5 then 700, 0.5					98.08	
Bic-Dm		600,3					92.69	
Bic-PP		600, 3					93.05	
ZrO_2/BLA	(600, 4)[c]	400, 4	12	15:1	2[a]	50	89.99	15
KNO_3/OSA		700, 4	10	45:1	2	65	100	32
Li_2CO_3-PHA	(900, 2)[c]	blending	5	12:1	4	65	98.4	64
CaO/FA	(1000, 4)[b]	1000, 2	1	6.9:1	5	70	96.97	65
KNO_3/FA		500, 5	8	15:1	15	170[d]	87.5	66
MLA	(500, 2)[b]		6	6:1	2	65	86.7	68

[a]Microwave-assisted reaction. BD: biodiesel yield, CL: catalyst loading, MOMR: methanol/oil molar ratio, PHA: peanut husk ash, Rt: reaction time, RT: reaction temperature, OSA: oil shale ash, FA: fly ash, BLA: bamboo leaf ash, and MLA: moringa leaf ash. [b]Calcination condition during active site preparation. [c]Calcination condition during the active site support preparation. [d]Reaction in autoclave.

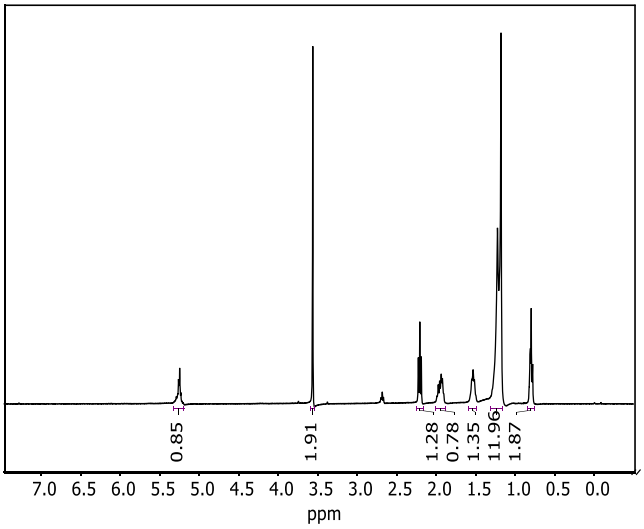

Figure 8. ^{1}H NMR spectrum of the WFOME produced using the C-Mix catalyst.

matched with the proton range from the methyl ester group ($-COOCH_3$) that appeared at around 3.57 ppm. This signal revealed the formation of WFOME. Additionally, $-CH_2$ protons at 2.23 ppm were employed to assess the conversion of WFO to its methyl esters. The carbon chain's methylene proton, the carbonyl methylene proton, and the degree of unsaturation displayed signals at 1.23, 1.51, and 5.26 ppm, respectively. The proper removal of glycerol from the WFOME can be observed by the absence of a peak at 4.16 ppm. The absence of signals between 4.08 and 4.28 ppm (glycerol moiety protons of the WFO) was due to the nearly complete conversion of triglycerides to WFOME.[9] The conversion of fatty acids into methyl esters was estimated by eq 8.[32]

$$X(\%) = \left(\frac{2\beta}{3\alpha}\right) \times 100 \quad (8)$$

where X (%) is the conversion of triglycerides of WFO to its fatty acid methyl ester, β is the integral value of methoxy protons of methyl ester, and α is the integral value of the α-methylene protons of methyl ester.

The maximum WFO conversion in this study using ^{1}H NMR analysis (Figure 8) is 99.5% and belongs to the C-Mix catalyst-assisted transesterification. The reaction condition was a temperature of 65 °C, a reaction time of 1 h, a catalyst loading of 5 wt %, and a methanol to WFO molar ratio of 15:1.

Effect of Transesterification Parameters on WFO to WFOME Conversion. To analyze the effectiveness of various catalysts with various reaction variables, several factors were considered, such as the impact of catalyst loading (1 to 9 wt %), methanol-to-oil ratio (9:1 to 21:1), reaction time (20 to 120 min), and reaction temperature (35 to 75 °C). One variable at a time was investigated, as presented in Figure 9.

Effect of Reaction Temperature on Catalyst Performance. The performance of the catalysts was assessed using WFO transesterification. The impact of the reaction temperature is shown in Figure 9a. This study examined the response of all catalysts to temperature variations between 35 and 75 °C for 1.13 h reaction time using a molar ratio of 13.55:1 and catalyst loading of 5.42 wt %. The WFOME content increased with the increase in reaction temperature. Because it is within the range of the methanol's boiling point, the temperature for the maximum WFOME yield was between 55 and 65 °C. The WFOME content appears to decrease when the temperature rises above 65 °C. These phenomena were mentioned in some earlier published research as well for both alkali[8] and bifunctional[12] catalysts. At low reaction temperatures, the viscosity of the reaction mixture is higher, which makes the contact between the catalyst and reactants inadequate. However, because of liquid phase changes at higher temperatures, the biodiesel yield and ester concentration may decrease. Furthermore, the cost of production will increase as the temperature rises.[12] The largest WFOME yield was for C-Mix catalysis up to 65 °C most probably because of its higher alkalinity.[1] However, at a higher temperature, the C-Mix performance was lower. This may be due to a higher concentration of active sites in the reaction mixture because of leaching.[9] At reaction temperatures below 65 °C, the catalyst performance was directly proportional to their alkalinity. According to reports, alkalinity has a major role in the performance of catalysts during alkali transesterification.[1]

Effect of Reaction Time on Catalyst Performance. Figure 9b displays the impact of the reaction time on the WFOME yield for each catalyst. The reaction time ranged from 20 to 120 min, whereas other parameters are fixed at temperature of 65 °C using a molar ratio of 13.55:1 and catalyst loading of 5.42 wt %. According to Figure 9b, the catalyst amount of 5.42 wt % caused the WFOME content to rise during the first 20 min and reach as high as 76.05, 83.03, 72.55, and 73.45% for

https://doi.org/10.1021/acsomega.3c08108
ACS Omega 2024, 9, 2815−2829

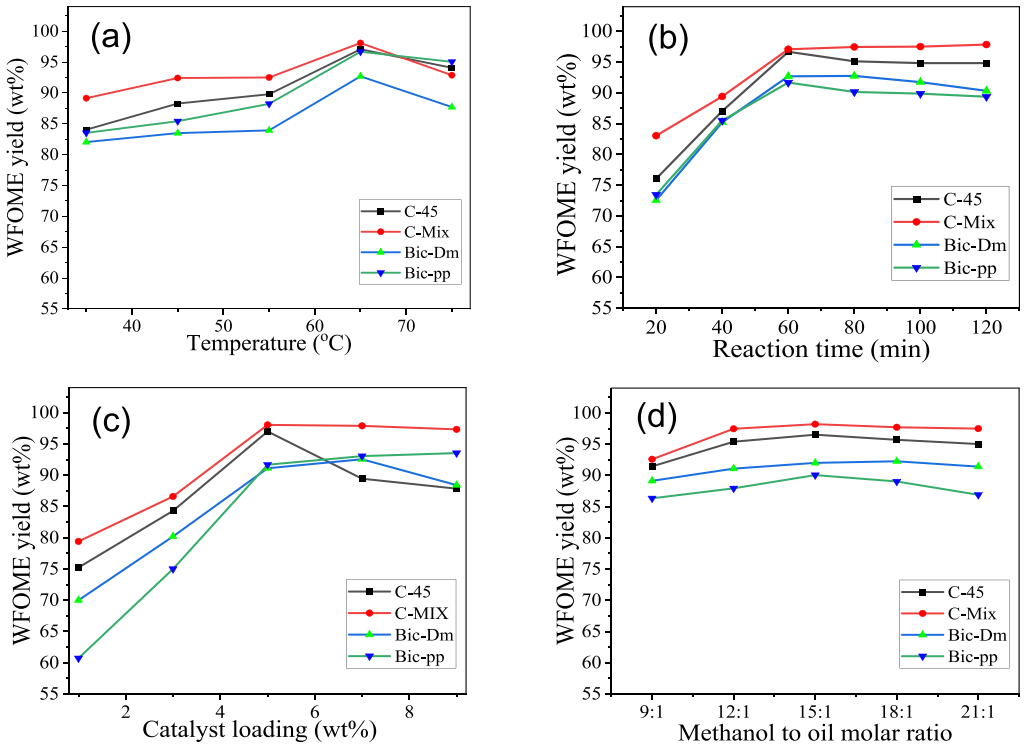

Figure 9. Effect of WFO transesterification reaction parameters: (a) reaction temperature, (b) reaction time, (c) catalyst loading, and (d) methanol to oil molar ratio on WFOME yield.

the catalysts C-45, C-Mix, Bic-Dm, and Bic-PP, respectively. Further, with an increase in the reaction duration to 60 min, the WFOME content reached and remained almost constant as a result of near-equilibrium conditions at 96.68, 97.08, 92.69, and 91.67% for C-45, C-Mix, Bic-Dm, and Bic-PP, respectively. The WFOME content decreases with a longer reaction time, possibly due to the reversibility of the transesterification reaction.[1]

Effect of Catalyst Loading on Catalyst Performance. The catalyst loading ranged from 1 to 9 wt % at a fixed reaction time (1 h) for a temperature of 65 °C using a molar ratio of 13.55:1. Results regarding the impact of catalyst quantity on catalytic activity are shown in Figure 9c. The quantity of catalyst utilized in this investigation had an impact on the transesterification. By increasing the amount of alkali catalyst from 1 to 5%, the content of WFOME increased from 75.23 to 97 and 79.4 to 98.08 (wt %) for C-45 and C-Mix, respectively. The WFOME yield at 1 wt % of Bic-Dm and Bic-PP was 70 and 61 wt %, respectively, and it reached 92.69 and 93.05 wt % at 7 wt % of catalyst loading. Therefore, the optimal catalyst loading is 5 and 7 wt % for alkali and bifunctional catalysts, respectively. This is because the possibility of an interaction between the catalyst and the reactant directly influences the rate of the reaction. Further increasing of the catalyst loading showed different effects, which may be a combination of higher active site concentration and inadequate stirring speed while the solution became more viscous.[8]

Effect of Methanol to Oil Molar Ratio on Catalyst Performance. The molar ratio of methanol and oil is one of the important variables that affects the transesterification reaction. According to stoichiometry, 3 mol of methanol is needed for every mole of WFO, and an excess of the methanol will cause the equilibrium to shift in favor of the WFOME production. However, the extra methanol must be recovered and removed from the WFOME, which drives up the cost of production. Therefore, the increase in the process expense must be taken into account while choosing an optimal molar ratio. Figure 9d shows the response of WFOME yield to methanol to oil molar ratios of 9:1, 12:1, 15:1, 18:1, and 21:1 for a 1 h reaction time at a temperature of 65 °C using a catalyst loading of 5 wt % (for C-45 and C-mix) and 7 wt % (for Bic-Dm and Bic-PP). The maximum WFOME yield was obtained when the methanol/oil molar ratio is raised to 15:1 (Table 5). The WFOME content cannot be raised by adding more methanol. This is due to glycerol's solubility in methanol and methanol in biodiesel, which causes the equilibrium concentration of glycerol in biodiesel to increase in response to the unnecessary excess methanol. This makes the separation of WFOME and glycerol difficult. Additionally, the methanol removal process becomes more complex.[67]

A comparison of alkali and bifunctional catalysts for the production of biodiesel is shown in Table 5. These catalysts were synthesized by impregnating various ash supports, such as bamboo leaf ash (BLA), oil shale ash (OSA), peanut husk ash (PHA), and fly ash (FA), with different active site precursors for alkali and bifunctional catalysts. When compared to the catalysts listed in Table 5, the catalyst created in this study performed better than the majority of them in terms of reaction speed and oil-to-methyl ester conversion.

Turnover Frequency of Catalysts. Because heterogeneous catalysts usually have different surface areas and pore sizes, judging their activity with the biodiesel yield only will be misleading. This can be eliminated by measuring catalysts' turnover frequency (TOF).[69] The TOFs of catalysts were found to be 21.79, 16.31, 24.96, and 17.65 h^{-1} for C-45, C-Mix, Bic-Dm, and Bic-PP catalysts, respectively. These results reveal that Bic-Dm had the highest TOF, indicating its highest efficiency during the WFO transesterification reaction.[54] This

https://doi.org/10.1021/acsomega.3c08108
ACS Omega 2024, 9, 2815−2829

may be associated with its highest BET surface area (Table 4) as compared to the other catalysts in the present study.[69] A similar observation was reported for Al_2O_3 supported CaO catalysts with TOFs of 100.8 and 43.2 h^{-1}.[69] On the other hand, the lowest TOF belongs to the C-Mix catalyst even though it had the highest WFOME yield (98.08 wt %). Lower TOFs of peduncle burnt ash (9.13 h^{-1})[31] and acai seed ash catalyst (4.90 h^{-1})[54] were reported in the literature as compared to catalysts in this study.

Moisture Resistance of the Catalysts. The presence of water and free fatty acids makes the alkali catalytic process challenging. Triglycerides will hydrolyze into free fatty acids and glycerol in the presence of water, promoting the production of soap. This impedes the separation of biodiesel and glycerin and decreases the biodiesel yield.[70] The performance of catalysts in response to 5 wt % moisture content was examined in this study, and the result is presented in Figure 10. The C-Mix catalyst assisted WFO trans-

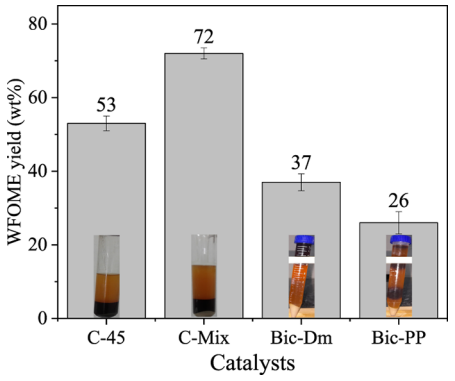

Figure 10. Catalysts' performance under an additional 5 wt % moisture content in WFO.

esterification process was less sensitive to the presence of water as compared to the other catalysts in this study. The result may be attributed to the presence of silica in the C-Mix (Figure 6), which absorbs the water molecules.[71] The biodiesel yield dropped from 98.08 to 72 wt % with 5 wt % additional water in the form of moisture. The performance drop was much lower than the reported value for a bare potassium silicate catalyst (98.2 to 40 wt %).[8] The performance of catalysts in the presence of 5 wt % water then followed the order C-45 > Bic-Dm > Bic-PP with a WFOME yield of 53, 45, and 32 wt %, respectively. The C-45 catalyst's better moisture resistance might be explained by its hydrophobic character as a result of the unburned char in it. Hydrophobicity prevents the deactivation of active sites in a polar environment.[72] Lewis acids are sensitive to moisture, which may account for the poor performance of the bifunctional catalysts.[72] That may be the reason the bifunctional catalysts showed low moisture resistance. When the water-added WFO was transesterified using Bic-Dm, the majority of the excess methanol and contaminants were separated into the upper phase (Figure 10). The bottom phase could be a mixture of WFOME, monoglycerides, diglycerides, and triglycerides.[73] For the Bic-PP-assisted transesterification of water-mixed WFO (Figure 10), more than two heterogeneous phases were observed.

Catalysts' Reusability. When a catalyst is used on an industrial scale, its capacity to be reused is quite important. A reusability test was performed for both recovered and regenerated forms of spent catalysts. The spent catalysts were recovered by solvent washing followed by oven drying. Regeneration was conducted via the recalcination of the recovered catalysts. The recovered catalysts were designated by C-r_i and the regenerated ones by C-r_{ci} (Figure 11). The letter

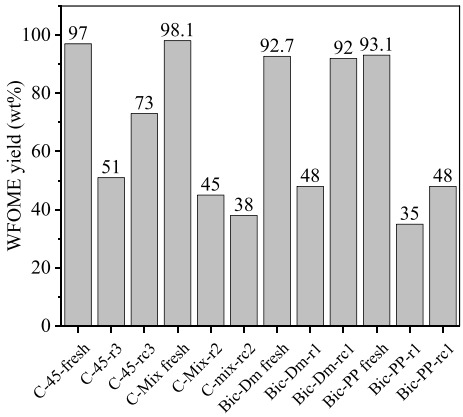

Figure 11. Catalyst reusability after recovery and regeneration

"C" stands for the catalysts (C-45, C-Mix, Bic-Dm, or Bic-PP), r stands for the recovered catalyst, and r_c stands for regenerated catalysts. The subscript "*i*" denotes both the reuse cycle and regeneration being performed after a catalyst was recovered and was ready for the "*i*th" reuse cycle. The recovered C-45 catalyst showed the best potential for reuse, yielding 80.68, 64.42, and 51 wt % of WFOME for the first (C-45-r_1), second (C-45-r_2), and third (C-45-r_3) cycles, respectively. However, the WFOME drastically dropped from 98.08 to 45 wt % when the recovered C-Mix catalyst (C-Mix-r_2) was employed during the transesterification reaction. The WFOME yields declined significantly from 92.69 and 93.05 wt % to 48 and 35 wt %, respectively, for the recovered Bic-Dm (Bic-Dm-r_1) and Bic-PP (Bic-PP-r_1) catalysts used as a first cycle reuse. The reusability result shows that the recovered catalyst from C-45 has the best catalytic performance as compared to that of the catalyst recovered from C-Mix, Bic-Dm, and Bic-PP during transesterification of WFO (Figure 11). The presence of char in the C-45 may be one of the reasons for its higher reusability because the char induces catalyst hydrophobicity, facilitating the preferential adsorption of triglycerides and preventing the deactivation of active sites in a polar environment.[72] The presence of char may also slow the active site leaching process from C-45 via steric hindrance that slows the vulnerability of the active sites for leaching. The C-Mix and bifunctional catalysts probably lack these properties. The kind and makeup of the compounds in the catalysts structure were also potential reasons for the difference in the reusability.[17]

The effect of regeneration using calcination of recovered catalysts was analyzed for the catalyst yielding less WFOME (Figure 11). The WFOME yields were increased from 51 to 73, 48 to 92, and 35 to 48 wt % on regeneration of C-45-r_3, Bic-Dm-r_1, and Bic-PP-r_1 catalysts, respectively. However, the yield of WFOME was reduced when the regenerated C-Mix-r_2 (i.e., C-Mix-r_{2c}) was employed in the transesterification of WFO as compared to the recovered catalyst (C-Mix-r_2). This may be due to the sintering and agglomeration of the metallic silicate in the C-Mix catalyst.[61] Further, the results were confirmed by using FTIR analysis (Figure 12).

https://doi.org/10.1021/acsomega.3c08108
ACS Omega 2024, 9, 2815−2829

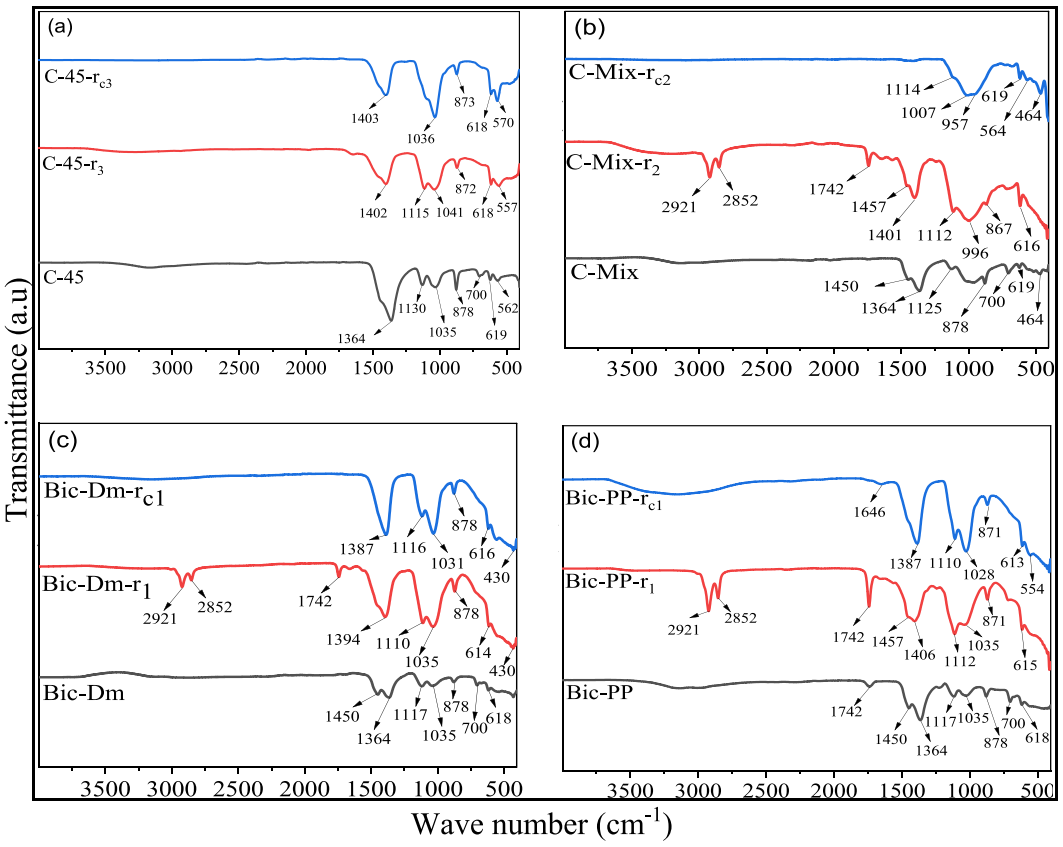

Figure 12. FTIR spectra of catalyst at different reuse cycles: (a) C-45, (b) C-Mix, (c) Bic-Dm, and (d) Bic-PP.

Using FTIR analysis of fresh, recovered, and regenerated catalysts (Figure 11), it was attempted to elucidate the catalyst deactivation mechanism. The FTIR spectrum interpretation of the reused catalysts is identical to that of fresh catalysts (Figure 5) with a few differences, for example, at 2921 and 2852 cm^{-1}. These bands did not appear in the FTIR spectrum of the C-45 catalyst, which was ready for reuse (Figure 12a). The peaks at wavenumbers 2921 and 2852 cm^{-1} represent the C−H bond vibrations and demonstrate that the catalyst recovery procedure was ineffective in removing organic compounds (triglycerides and glycerol) from the catalyst surface (Figure 12b−d). Further, the color observation shows that the spent catalyst becomes dark in color, which also reveals the presence of the organic compounds on the surface of the recovered catalysts.[74] This contamination reduces the density of active sites and causes catalyst deactivation.[74,75] The C-45-r$_3$ FTIR spectrum mimics that of the carbonated hydroxyapatite in its as-prepared state as reported by Zhou et al.[76] This most likely occurred as a result of the leaching of the other carbonates that had previously obscured the carbonated hydroxyapatite, not revealing its characteristic FTIR spectrum. The weakening of the C−O and metal−O vibration bands and the rise in the PO_4^{3-} vibration intensities for C-45-r$_3$ compared to C-45 were indicators of the carbonate leaching (Figure 12a). As can be seen from the C-45-r$_{c3}$ FTIR spectrum, the recalcination of C-45-r$_3$ resulted in the recrystallization of compounds, and the WFOME yield reached 78 wt % (Figure 11). The same phenomena were observed for the C-Mix-recovered catalyst (C-Mix-r$_2$). But when C-Mix-r$_2$ was recalcined (C-Mix-r$_{c2}$), new phenomena appeared, including the removal of the CO_3 bending band at 878 cm^{-1} and the C−O bond vibrations at 1401 and 1457 cm^{-1}. Only bands corresponding to Si−O−Si and Si−O vibrations were observed, which may be due to a reaction of metallic carbonates with silica to form metallic silicates. There was a transition from the light gray color of C-Mix-r$_2$ to the light green C-Mix-rc$_2$ during the regeneration process that gives supportive information for this phenomenon. This chemical change may reduce the catalyst activity in two different ways: the formation of more stable compounds (certain stable compounds have lower catalytic activity[8]) and the chemical change that could cause eutectic melting and sintering, which reduces the accessibility of active sites.[61] Bic-Dm and Bic-PP catalysts have nearly similar FTIR patterns, except for a few differences. The pattern shows that there is leaching of the active sites, especially in alkali metal carbonates. However, in their recovered and regenerated version, the catalyst Bic-Dm performed better than Bic-PP. This is probably due to surface active site poisoning of the Bic-PP catalyst with products, reactants, or both in addition to active site leaching.[77]

CONCLUSIONS

The alkali and bifunctional catalysts containing heterogeneous active sites were derived from composites of lignocellulosic biomass (LB) ash, and chemical sources were efficient for the waste frying oil methanolysis. The alkalinity of the catalysts played a primary role in affecting their activity. That is, a higher catalyst alkalinity offered a higher WFOME yield. The alkali catalysts obtained their strong alkalinity due to the presence of single and double alkali metallic carbonates in their structure. The carbonates were also accompanied by strong alkali metallic oxides such as CaO and K_2O. In addition to the metallic carbonates and oxides, the bifunctional catalysts

https://doi.org/10.1021/acsomega.3c08108
ACS Omega 2024, 9, 2815−2829

contained the Lewis acid site source t-ZrO_2 and the alkali C-Mix catalyst K_2SiO_3. The compositional change caused the bifunctional catalysts to have relatively lower alkalinity. The highest alkalinity was for C-Mix due to its lower unburned char content compared to C-45. Differences in catalyst texture and crystallinity also possibly induced the activity difference. The results indicated that the combustion performance of LBs and catalyst composite materials (CCMs) had a great impact on the physicochemical properties of catalysts. The maximum WFOME yields were 98.08, 97, 93.05, and 92.69 wt % for C-Mix, C-45, Bic-PP, and Bic-Dm catalyst, respectively. The TOF results were found to be in the order of Bic-Dm (24.96 h^{-1}), C-45 (21.79 h^{-1}), Bic-PP (17.65 h^{-1}), and C-Mix (16.31 h^{-1}). The reusability of the catalyst was better for alkali catalysts and better for the C-45 catalyst. The highest WFOME yield of 92 wt % was obtained for the regenerated Bic-Dm catalyst during the reusability test. The C-Mix catalyst had a high tolerance to an additional 5 wt % water into WFO, and the yield of WFOME was 72 wt %. The overall result shows that the catalysts that were derived from LBs and chemical precursor composites are promising heterogeneous catalysts for biodiesel production as green, low-cost, and renewable materials. However, further investigation is recommended to develop strategies to increase the rate of reuse of the catalysts.

AUTHOR INFORMATION

Corresponding Author

Nurelegne Tefera Shibeshi − *School of Chemical and Bioengineering, Addis Ababa Institute of Technology, Addis Ababa University, Addis Ababa 1176, Ethiopia;* orcid.org/0000-0002-4387-4889; Email: nurelegne.tefera@aait.edu.et

Authors

Demelash Tilahun Bekele − *Department of Chemical Engineering, College of Engineering, Addis Ababa Science and Technology University, Addis Ababa 16417, Ethiopia;* orcid.org/0000-0002-4118-6759

Ali Shemsedin Reshad − *Department of Chemical Engineering, College of Engineering and Center of Excellence for Sustainable Energy Research, Addis Ababa Science and Technology University, Addis Ababa 16417, Ethiopia;* orcid.org/0000-0003-3695-954X

Complete contact information is available at: https://pubs.acs.org/10.1021/acsomega.3c08108

Funding

This study was funded by the Addis Ababa Science and Technology University as PhD student dissertation work.

Notes

The authors declare no competing financial interest.

ACKNOWLEDGMENTS

The authors would like to express their special thanks to the Chemical and Food Process Engineering laboratories under the Chemical Engineering Department, Addis Ababa Science and Technology University, Ethiopia, for providing various analytical facilities and sample analysis. Further, the first author would like to thank the Addis Ababa Science and Technology University for giving fellowship opportunity for PhD study.

ACRONYMS LIST

A/C: char prepared from coffee husk calcination at 600 °C for 2 h
AOCS: American Oil Chemists Society
ASTM: American Society for Testing and Materials
BET: Brunauer−Emmett−Teller
CCM: catalyst composite material
CH: coffee husk
CH−TS: coffee husk and *Eragrostis tef* (teff) straw blended biomass
DTA: differential thermal analysis
DTG: derivative thermogravimetric
FTIR: Fourier transform infrared spectroscopy
^{1}H NMR: proton nuclear magnetic resonance
ISO: International Organization for Standardization
LBs: lignocellulosic biomasses
mA/C: char prepared from coffee husk and *Eragrostis tef* (teff) straw blended biomass calcination at 600 °C for 2 h
SEM: scanning electron microscopy
TGA: thermogravimetric analysis
TOF: turnover frequency
TS: *Eragrostis tef* (teff) straw
WFO: waste frying oil
WFOME: waste frying oil methyl ester
XRD: X-ray diffraction
ZN: zirconyl nitrate monohydrate

REFERENCES

(1) Bekele, D. T.; Shibeshi, N. T.; Reshad, A. S. Heterogeneous catalysts from metallic oxides and lignocellulosic biomasses ash for the valorization of feedstocks into biodiesel: an overview. *BioEnergy Res.* **2023**, *16*, 1361−1379.

(2) Sahani, S.; Roy, T.; Chandra Sharma, Y. Clean and efficient production of biodiesel using barium cerate as a heterogeneous catalyst for the biodiesel production; kinetics and thermodynamic study. *J. Cleaner Prod.* **2019**, *237*, No. 117699.

(3) Mardhiah, H. H.; Ong, H. C.; Masjuki, H. H.; et al. A review on latest developments and future prospects of heterogeneous catalyst in biodiesel production from non-edible oils. *Renew Sustain energy Rev.* **2017**, *67*, 1225−1236.

(4) Yaşar, F. Biodiesel production via waste eggshell as a low-cost heterogeneous catalyst: Its effects on some critical fuel properties and comparison with CaO. *Fuel* **2019**, *255*, No. 115828.

(5) Lee, D. W.; Park, Y. M.; Lee, K. Y. Heterogeneous base catalysts for transesterification in biodiesel synthesis. *Catal. Surv from Asia* **2009**, *13*, 63−77.

(6) Abnisa, F.; Sanni, S. E.; Alaba, P. A. Comparative study of catalytic performance and degradation kinetics of biodiesels produced using heterogeneous catalysts from kaolinite. *J. Environ. Chem. Eng.* **2021**, *9*, No. 105569.

(7) Hanif, M. A.; Nisar, S.; Rashid, U. Supported solid and heteropoly acid catalysts for production of biodiesel. *Catal. Rev. - Sci. Eng.* **2017**, *59*, 165−188.

(8) Hindryawati, N.; Maniam, G. P.; Karim, M. R.; Chong, K. F. Transesterification of used cooking oil over alkali metal (Li, Na, K) supported rice husk silica as potential solid base catalyst. *Eng. Sci. Technol. an Int. J.* **2014**, *17*, 95−103.

(9) Bekele, D. T.; Shibeshi, N. T.; Reshad, A. S. (**2022**) KNO3-Loaded Coffee Husk Ash as a Heterogeneous Alkali Catalyst for Waste Frying Oil Valorization into Biodiesel. *ACS Omega.* 745129.

(10) Daimary, N.; Eldiehy, K. S. H.; Bora, N.; et al. Towards integrated sustainable biofuel and chemical production: An application of banana pseudostem ash in the production of biodiesel and recovery of lignin from bamboo leaves. *Chemosphere* **2023**, *314*, No. 137625.

(11) Sharma, M.; Khan, A. A.; Puri, S. K.; Tuli, D. K. Wood ash as a potential heterogeneous catalyst for biodiesel synthesis. *Biomass and Bioenergy* **2012**, *41*, 94−106.
(12) Mansir, N.; Teo, S. H.; Mijan, N. A.; Taufiq-Yap, Y. H. Efficient reaction for biodiesel manufacturing using bi-functional oxide catalyst. *Catal. Commun.* **2021**, *149*, No. 106201.
(13) Kedir, W. M. Bifunctional Heterogeneous Catalysts for Biodiesel Production Using Low-Cost Feedstocks: A Future Perspective. *Adv. Biodiesel* **2023**, 285 DOI: 10.5772/intechopen.109482.
(14) Booramurthy, V. K.; Kasimani, R.; Pandian, S.; Ragunathan, B. Nano-sulfated zirconia catalyzed biodiesel production from tannery waste sheep fat. *Environ. Sci. Pollut Res.* **2020**, *27*, 20598−20605.
(15) Fatimah, I.; Rubiyanto, D.; Taushiyah, A.; et al. Use of ZrO2 supported on bamboo leaf ash as a heterogeneous catalyst in microwave-assisted biodiesel conversion. *Sustain Chem. Pharm.* **2019**, *12*, No. 100129.
(16) Parghi, K. D.; Kale, S. R.; Kahandal, S. S.; et al. Sequential synthesis of *β*-amino alcohols using a CeO 2-ZrO2 bifunctional catalyst system. *Catal. Sci. Technol.* **2013**, *3*, 1308−1313.
(17) Abdul Mutalib, A. A.; Ibrahim, M. L.; Matmin, J.; et al. SiO2-Rich Sugar Cane Bagasse Ash Catalyst for Transesterification of Palm Oil. *Bioenergy Res.* **2020**, *13*, 986−997.
(18) Li, H.; Liu, F.; Ma, X.; et al. Catalytic performance of strontium oxide supported by MIL−100 (Fe) derivate as transesterification catalyst for biodiesel production. *Energy Convers Manag* **2019**, *180*, 401−410.
(19) Yao, D.; Yang, H.; Chen, H.; Williams, P. T. Co-precipitation, impregnation and so-gel preparation of Ni catalysts for pyrolysis-catalytic steam reforming of waste plastics. *Appl. Catal. B Environ* **2018**, *239*, 565−577.
(20) Reinmöller, M.; Sieradzka, M.; Laabs, M.; et al. Investigation of the thermal behaviour of different biomasses and properties of their low- and high-temperature ashes. *Fuel* **2021**, *301*, No. 121026.
(21) Ronda, A.; Della Zassa, M.; Gianfelice, G.; et al. Smouldering of different dry sewage sludges and residual reactivity of their intermediates. *Fuel* **2019**, *247*, 148−159.
(22) Toptas, A.; Yildirim, Y.; Duman, G.; Yanik, J. Combustion behavior of different kinds of torrefied biomass and their blends with lignite. *Bioresour. Technol.* **2015**, *177*, 328−336.
(23) Wongmat, Y.; Wagner, D. R. Effect of Potassium Salts on Biochar Pyrolysis. *Energies* **2022**, *15*, 5779.
(24) Amibo, T. A.; Beyan, S. M.; Damite, T. M. Production and optimization of bio-based silica nanoparticle from teff straw (eragrostis tef) using RSM-based modeling, characterization aspects, and adsorption efficacy of methyl orange dye. *J. Chem.* **2022**, *2022*, 1−15.
(25) Reshad, A. S.; Tiwari, P.; Goud, V. V. Extraction of oil from rubber seeds for biodiesel application: Optimization of parameters. *Fuel* **2015**, *150*, 636−644.
(26) Nath, B.; Kalita, P.; Das, B.; Basumatary, S. Highly efficient renewable heterogeneous base catalyst derived from waste Sesamum indicum plant for synthesis of biodiesel. *Renew Energy* **2020**, *151*, 295−310.
(27) Fraile, J. M.; García, N.; Mayoral, J. A.; et al. The basicity of mixed oxides and the influence of alkaline metals: The case of transesterification reactions. *Appl. Catal. A Gen* **2010**, *387*, 67−74.
(28) Song, Y.; Liu, J.; Evrendilek, F.; et al. Combustion behaviors of Pteris vittata using thermogravimetric, kinetic, emission and optimization analyses. *J. Clean Prod* **2019**, *237*, No. 117772.
(29) Liu, J.; Jiang, X.; Cai, H.; Gao, F. Study of combustion characteristics and kinetics of agriculture briquette using thermogravimetric analysis. *ACS omega* **2021**, *6*, 15827−15833.
(30) Changmai, B.; Rano, R.; Vanlalveni, C.; Rokhum, L. A novel Citrus sinensis peel ash coated magnetic nanoparticles as an easily recoverable solid catalyst for biodiesel production. *Fuel* **2021**, *286*, No. 119447.
(31) Nath, B.; Basumatary, B.; Brahma, S.; et al. Musa champa peduncle waste-derived efficient catalyst: Studies of biodiesel synthesis, reaction kinetics and thermodynamics. *Energy* **2023**, *270*, No. 126976.
(32) Al-Hamamre, Z.; Sandouqa, A.; Al-Saida, B.; et al. Biodiesel production from waste cooking oil using heterogeneous KNO3/Oil shale ash catalyst. *Renew Energy* **2023**, *211*, 470−483.
(33) Ouanji, F.; Khachani, M.; Boualag, M.; et al. Large-scale biodiesel production from Moroccan used frying oil. *Int. J. Hydrogen Energy* **2016**, *41*, 21022−21029.
(34) Damanik, N.; Ong, H. C.; Chong, W. T.; Silitonga, A. S. Biodiesel production from Calophyllum inophyllum−palm mixed oil. *Energy Sources, Part A Recover Util Environ. Eff* **2017**, *39*, 1283−1289.
(35) Tan, C.-H.; Ghazali, H. M.; Kuntom, A.; et al. Extraction and physicochemical properties of low free fatty acid crude palm oil. *Food Chem.* **2009**, *113*, 645−650.
(36) EL-Sayed, S. A.; Mostafa, M. E. Kinetics, thermodynamics, and combustion characteristics of Poinciana pods using TG/DTG/DTA techniques. *Biomass Convers. Bioref.* **2021**, 11583.
(37) Putra, H. P.; Hilmawan, E.; Darmawan, A.; et al. Theoretical and experimental investigation of ash-related problems during coal co-firing with different types of biomass in a pulverized coal-fired boiler. *Energy* **2023**, *269*, No. 126784.
(38) de S. Barros, S.; Pessoa Junior, W. A. G.; Sá, I. S. C.; Takeno, M. L.; Nobre, F. X.; Pinheiro, W.; Manzato, L.; Iglauer, S.; de Freitas, F. A.; et al. Pineapple (Ananás comosus) leaves ash as a solid base catalyst for biodiesel synthesis. *Biores. Technol.* **2020**, *312*, No. 123569.
(39) Lang, Q.; Liu, Z.; Li, Y.; et al. Combustion characteristics, kinetic and thermodynamic analyses of hydrochars derived from hydrothermal carbonization of cattle manure. *J. Environ. Chem. Eng.* **2022**, *10*, No. 106938.
(40) Yang, X.; Zhao, Y.; Li, W.; et al. Unveiling the pyrolysis mechanisms of hemicellulose: experimental and theoretical studies. *Energy Fuels* **2019**, *33*, 4352−4360.
(41) Silva, K. G.; Assis, P. S. Combustibility behavior of PCI coals, green petroleum coke and charcoal fines used as fuel for injection into blast furnace tuyeres. *REM-International Eng. J.* **2019**, *72*, 125−131.
(42) Haykiri-Acma, H.; Yaman, S.; Kucukbayrak, S. Production of biobriquettes from carbonized brown seaweed. *Fuel Process. Technol.* **2013**, *106*, 33−40.
(43) Li, X.; Ma, B.; Xu, L.; et al. Thermogravimetric analysis of the co-combustion of the blends with high ash coal and waste tyres. *Thermochim. Acta* **2006**, *441*, 79−83.
(44) Li, Y.-H.; Lin, H.-T.; Xiao, K.-L.; Lasek, J. Combustion behavior of coal pellets blended with Miscanthus biochar. *Energy* **2018**, *163*, 180−190.
(45) Du, S.; Yang, H.; Qian, K.; et al. Fusion and transformation properties of the inorganic components in biomass ash. *Fuel* **2014**, *117*, 1281−1287.
(46) Bogush, A. A.; Stegemann, J. A.; Williams, R.; Wood, I. G. Element speciation in UK biomass power plant residues based on composition, mineralogy, microstructure and leaching. *Fuel* **2018**, *211*, 712−725.
(47) Monoi, T.; Sasaki, Y. Silica-supported Cr [N (SiMe3) 2] 3/ isobutylalumoxane catalyst for selective ethylene trimerization. *J. Mol. Catal. A Chem.* **2002**, *187*, 135−141.
(48) Prajapati, P.; Shrivastava, S.; Sharma, V.; et al. Karanja seed shell ash: A sustainable green heterogeneous catalyst for biodiesel production. *Results Eng.* **2023**, *18*, No. 101063.
(49) Basumatary, B.; Brahma, S.; Nath, B.; et al. Post-harvest waste to value-added materials: Musa champa plant as renewable and highly effective base catalyst for Jatropha curcas oil-based biodiesel production. *Bioresour Technol. Reports* **2023**, *21*, No. 101338.
(50) Choudhary, R.; Koppala, S.; Swamiappan, S. Bioactivity studies of calcium magnesium silicate prepared from eggshell waste by sol−gel combustion synthesis. *J. Asian Ceram Soc.* **2015**, *3*, 173−177.
(51) Yang, X.; Zhang, S. Characterizing and modeling the rheological performances of potassium silicate solutions. *J. Solution Chem.* **2016**, *45*, 1890−1901.

https://doi.org/10.1021/acsomega.3c08108
ACS Omega 2024, 9, 2815−2829

(52) Roschat, W.; Siritanon, T.; Yoosuk, B.; Promarak, V. Rice husk-derived sodium silicate as a highly efficient and low-cost basic heterogeneous catalyst for biodiesel production. *Energy Convers Manag* **2016**, *119*, 453−462.
(53) Prekajski, M.; Mirković, M.; Todorović, B.; et al. Ouzo effect—New simple nanoemulsion method for synthesis of strontium hydroxyapatite nanospheres. *J. Eur. Ceram Soc.* **2016**, *36*, 1293−1298.
(54) Mares, E. K. L.; Gonçalves, M. A.; da Luz, P. T. S.; et al. Acai seed ash as a novel basic heterogeneous catalyst for biodiesel synthesis: Optimization of the biodiesel production process. *Fuel* **2021**, *299*, No. 120887.
(55) Basumatary, B.; Basumatary, S.; Das, B.; et al. Waste Musa paradisiaca plant: An efficient heterogeneous base catalyst for fast production of biodiesel. *J. Clean Prod* **2021**, *305*, No. 127089.
(56) Rahman, N. J. A.; Ramli, A.; Jumbri, K.; Uemura, Y. Tailoring the surface area and the acid−base properties of ZrO2 for biodiesel production from Nannochloropsis sp. *Sci. Rep.* **2019**, *9*, 16223.
(57) Kaur, N.; Ali, A. Kinetics and reusability of Zr/CaO as heterogeneous catalyst for the ethanolysis and methanolysis of Jatropha crucas oil. *Fuel Process. Technol.* **2014**, *119*, 173−184.
(58) Olatundun, E. A.; Borokini, O. O.; Betiku, E. Cocoa pod husk-plantain peel blend as a novel green heterogeneous catalyst for renewable and sustainable honne oil biodiesel synthesis: A case of biowastes-to-wealth. *Renew Energy* **2020**, *166*, 163−175.
(59) SHI, G. l.; YU, F.; YAN, X. l.; LI, R. f. Synthesis of tetragonal sulfated zirconia via a novel route for biodiesel production. *J. Fuel Chem. Technol.* **2017**, *45*, 311−316.
(60) Arefiev, A. V.; Podborodnikov, I. V.; Shatskiy, A. F.; Litasov, K. D. Synthesis and Raman Spectra of K−Ca Double Carbonates: K 2 Ca (CO 3) 2 Bütschliite, Fairchildite, and K 2 Ca 2 (CO 3) 3 at 1 Atm. *Geochemistry Int.* **2019**, *57*, 981−987.
(61) Morris, J. D.; Daood, S. S.; Chilton, S.; Nimmo, W. Mechanisms and mitigation of agglomeration during fluidized bed combustion of biomass: A review. *Fuel* **2018**, *230*, 452−473.
(62) El-Maghraby, A.; Khaled, K. F.; Beherei, H. H.; El-Kheshen, A. A. *Synthesis and characterization of leucite nano-crystalline extracted from Saudi clay for dental application*; Trade Science Inc., 2012
(63) Sharikh, A. M.; Sulaiman, S.; Azmi, A. S.; Sulaiman, S. Z. (2018) Potassium carbonate from pineapple and orange peels as catalyst for biodiesel production. In: *AIP Conference Proceedings*. AIP Publishing LLC, p 020290.
(64) Dai, Y.-M.; Chen, K.-T.; Wang, Y.-J.; Chen, C.-C. Application of peanut husk ash as a low-cost solid catalyst for biodiesel production. *Int. J. Chem. Eng. Appl.* **2014**, *5*, 276.
(65) Chakraborty, R.; Bepari, S.; Banerjee, A. Transesterification of soybean oil catalyzed by fly ash and egg shell derived solid catalysts. *Chem. Eng. J.* **2010**, *165*, 798−805.
(66) Kotwal, M. S.; Niphadkar, P. S.; Deshpande, S. S.; et al. Transesterification of sunflower oil catalyzed by flyash-based solid catalysts. *Fuel* **2009**, *88*, 1773−1778.
(67) Dhawane, S. H.; Kumar, T.; Halder, G. Parametric effects and optimization on synthesis of iron (II) doped carbonaceous catalyst for the production of biodiesel. *Energy Convers Manag* **2016**, *122*, 310−320.
(68) Aleman-Ramirez, J. L.; Moreira, J.; Torres-Arellano, S.; et al. Preparation of a heterogeneous catalyst from moringa leaves as a sustainable precursor for biodiesel production. *Fuel* **2021**, *284*, No. 118983.
(69) Umdu, E. S.; Seker, E. Transesterification of sunflower oil on single step sol−gel made Al2O3 supported CaO catalysts: Effect of basic strength and basicity on turnover frequency. *Bioresour. Technol.* **2012**, *106*, 178−181.
(70) Miyuranga, K. A. V.; Arachchige, U. S. P. R.; Marso, T. M. M.; Samarakoon, G. Biodiesel Production through the Transesterification of Waste Cooking Oil over Typical Heterogeneous Base or Acid Catalysts. *Catalysts* **2023**, *13*, 546.
(71) Yang, R.; Su, M.; Zhang, J.; et al. Biodiesel production from rubber seed oil using poly (sodium acrylate) supporting NaOH as a water-resistant catalyst. *Bioresour. Technol.* **2011**, *102*, 2665−2671.
(72) Refaat, A. A. Biodiesel production using solid metal oxide catalysts. *Int. J. Environ. Sci. Technol.* **2011**, *8*, 203−221.
(73) Botti, R. F.; Innocentini, M. D. M.; Faleiros, T. A.; et al. Biodiesel processing using sodium and potassium geopolymer powders as heterogeneous catalysts. *Molecules* **2020**, *25*, 2839.
(74) Aleman-Ramirez, J. L.; Moreira, J.; Torres-Arellano, S.; et al. Preparation of a heterogeneous catalyst from moringa leaves as a sustainable precursor for biodiesel production. *Fuel* **2021**, *284*, No. 118983.
(75) Gouran, A.; Aghel, B.; Nasirmanesh, F. Biodiesel production from waste cooking oil using wheat bran ash as a sustainable biomass. *Fuel* **2021**, *295*, No. 120542.
(76) Zhou, W. Y.; Wang, M.; Cheung, W. L. Selective laser sintered poly (L-lactide)/carbonated hydroxyapatite nanocomposite scaffolds: a bottom-up approach. *Adv Divers Ind Appl Nanocomposites*, Reddy, BSR, Ed, IntechOpen 2011 203−230.
(77) Oueda, N.; Bonzi-Coulibaly, Y. L.; Ouédraogo, I. W. K. Deactivation processes, regeneration conditions and reusability performance of CaO or MgO based catalysts used for biodiesel production—a review. *Mater. Sci. App.* **2017**, *8*, 94−122.

https://doi.org/10.1021/acsomega.3c08108
ACS Omega 2024, 9, 2815−2829